ACS Catalysis

Research Article

pubs.acs.org/acscatalysis

Highly Enhanced Photoactivity of Anatase TiO_2 Nanocrystals by Controlled Hydrogenation-Induced Surface Defects

Xiaomei Yu, Boseong Kim, and Yu Kwon Kim*

Department of Energy Systems Research and Department of Chemistry, Ajou University, Suwon 443-749, South Korea

Supporting Information

ABSTRACT: Anatase TiO_2 nanocrystals ($aTiO_2$) of a uniform size have been synthesized and were subject to a successive hydrogenation under a H_2 gas flow at elevated temperatures (500−700 °C). We found that the concentration of Ti^{3+} defects, such as Ti^{3+} interstitials and oxygen vacancies, and their distribution between surface and bulk varied significantly, depending on the hydrogenation temperature and time. Such changes in defects were found to be critical in enhancing the photoactivity of the hydrogenated TiO_2 (H-$aTiO_2$) by an order of magnitude. In our case, H-$aTiO_2$ nanocrystals hydrogenated at 600 °C for longer than 10 h showed 10 times higher photoactivity than $aTiO_2$, which was explained from a high surface-to-bulk defect ratio and a nonuniform distribution of defects between bulk and surface due to a preferential diffusion of bulk defects to the surface. Our study showed that a kinetically controlled hydrogenation condition could be used not only to control the surface/bulk defects but also to enhance the photoactivity of oxide nanocrystals.

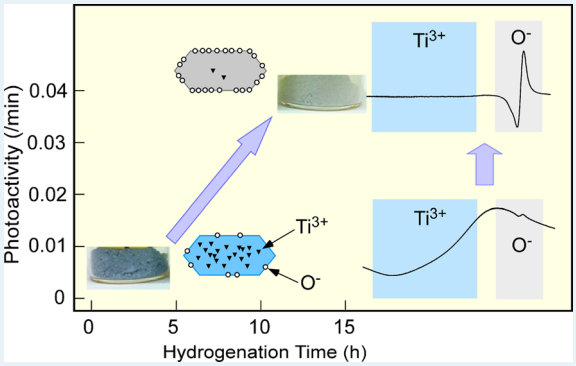

KEYWORDS: *anatase TiO_2 nanocrystal, oxygen vacancy, Ti^{3+}, defects, photoactivity, hydrogenation*

1. INTRODUCTION

TiO_2 is an attractive material as a photoactive material that can be applied to photocatalytic applications such as removal of organic contaminants and production of hydrogen.[1,2] However, the use of TiO_2 as a photocatalyst has been hampered by several obstacles, such as a high photoabsorption barrier due to the wide band gap (3.2 eV) of TiO_2[3] and a facile recombination of photogenerated electron/hole pairs[4] largely due to the presence of surface and bulk defects.[5] Attempts to overcome such problems have initiated many different approaches, including doping metals[6] or nonmetal elements,[7−9] controlling the shape and size of nanocrystals,[10−19] and introducing defects into nanocrystals.[20,21]

Recently, the role of different crystal facets in photocatalysis has been recognized, and it has initiated an attempt to control the shape of TiO_2 into the one surrounded with highly photoactive facets.[10,11,22] TiO_2 nanocrystals of different shapes with a varying fraction of {001} facets[12,23,24] have been obtained using F as a surfactant.[12] A higher photoactivity of the {001} facets of anatase TiO_2 than {101} has been attributed to a higher surface energy and unsaturated Ti_{5c} sites located on the {001} facets;[10,22] however, the facet-dependent photoactivity has been also shown to be modified by the influence of a surfactant such as fluorine in a way either to enhance or to reduce photoactivity.[12,22,25]

Hydrogenation of TiO_2 nanocrystals has also been proposed as a method of enhancing photoactivity.[26−29] Hydrogenated TiO_2 nanocrystals with a disordered surface structure have been shown to have an extended light absorption (down to a near-infrared region)[26] and a higher photocatalytic water splitting ability.[29] Hydrogenation of TiO_2 nanosheets with {001} facets performed under a high-pressure hydrogen atmosphere has been shown to induce an enhanced photoactivity of the TiO_2 nanosheets, and the origin was attributed to an increase in defects such as Ti^{3+} and oxygen vacancies in the bulk.[28]

However, the exact role of defects in the enhanced photoactivities of hydrogenated TiO_2 has been explained in widely different ways, which could be in part attributed to the complicated nature of defects.[30] The enhanced photocatalytic activities of hydrogenated TiO_2 have been attributed to the role of surface Ti−H bonds in improving optical absorption and an efficient photogenerated electron−hole separation.[28,31] In other cases, higher photoactivities of reduced TiO_2 nanocrystals have been attributed to the presence of Ti^{3+} or oxygen vacancies.[21,26] A high concentration of Ti^{3+} has been suggested to be important in producing a facile transfer of an electron or hole.[32] For the case of reduced TiO_2 nanoparticles prepared from TiH_2 as a precursor, paramagnetic oxygen vacancies have been identified as beneficial in enhancing the photoactivity.[33] In certain cases, a reduced photoactivity of hydrogenated TiO_2 has also been reported, and it was attributed to the role of bulk defects introduced.[34] In addition to the bulk defects (Ti^{3+} and an oxygen vacancy), the formation of surface chemical bonds, such as Ti−H, O−H, and even O_2-derived species on its surface

Received: July 18, 2013
Revised: September 15, 2013
Published: September 20, 2013

   dx.doi.org/10.1021/cs4005776 | ACS Catal. 2013, 3, 2479−2486

has been reported to tune the resulting photocatalytic activities.[28,31,35]

In this study, such complicated roles of surface and bulk defects were further examined by investigating changes of defects in anatase TiO_2 during hydrogenation processes. A successive treatment of TiO_2 with H_2 at an elevated temperature has turned out to provide a chance to probe the role of concentration and distribution of defects in enhancing photoactivity.

For such a purpose, we synthesized anatase TiO_2 nanosheets ($aTiO_2$) of a uniform size following the procedure employing HF as a surfactant.[11,12] The as-synthesized $aTiO_2$ was then subject to a successive hydrogenation under an atmospheric H_2 flow at 500−700 °C, which procedure resulted in hydrogenated TiO_2 nanocrystals (H-$aTiO_2$) with varying colors. We observed a greatly enhanced photoactivity for H-$aTiO_2$ prepared at 600 °C, under which condition a high concentration of Ti^{3+} in the bulk at the early stage of hydrogenation gradually transformed into surface oxygen vacancies (which produced O^- species as a result of O_2 at ambient conditions). Our results suggest that not just the absolute defect concentration but also a high surface-to-bulk ratio of defects is important in enhancing the photoactivity.[36]

2. EXPERIMENTAL DETAILS

Synthesis of Anatase TiO_2 Nanosheets ($aTiO_2$). A 25 g portion of tetrabutyl titanate was added into 25 mL of butanol in a Teflon beaker, then 4 mL of HF was added dropwise with a vigorous stirring into the beaker, placed in an ice bath. The resulting mixture was aged at room temperature (RT) and was subsequently transferred into an autoclave which maintained at 200 °C for 24 h. After the autoclave was cooled to RT, the TiO_2 precipitates were filtered and rinsed with deionized water. After drying at 60 °C for 6 h, white anatase TiO_2 powders were obtained. The surface area of our $aTiO_2$ (as-synthesized) was determined to be ∼40 m^2/g from a BET measurement, which was quite close to that of p-25 (∼47 m^2/g, measured in our lab).

Hydrogenation of $aTiO_2$. Hydrogenation was performed under a H_2 gas flow (50 sccm) at atmospheric pressure while the TiO_2 nanocrystals were placed in a quartz tube maintained at an elevated temperature in the range of 500−700 °C. A successive hydrogenation for a fixed period of time (0.5−1 h) was performed on $aTiO_2$, resulting in a gradual color change from white ($aTiO_2$) to blue, then finally to gray, as shown in Figure 1.

Characterization of $aTiO_2$ and H-$aTiO_2$. The X-ray diffraction (XRD) spectra were obtained from an X-ray diffractometer (Rigaku, Ultima III) using Cu Kα (λ = 0.154 06 nm) to examine the bulk crystalline structure and the size of our TiO_2 nanocrystals. The morphology and structure of our $aTiO_2$ and H-$aTiO_2$ were observed by a field emission transmission electron microscope (FEI Tecnai G2 F30 S-Twin). UV−vis diffuse reflectance (DR) spectroscopy measurements were performed on a UV-DR spectrometer (Scinco, Neosys-2000) equipped with an integrating sphere, and $BaSO_4$ was used as the reference to obtain absorption spectra for the determination of the band gap. Raman spectra were measured using an inVia Raman microscope (Renishaw) with a laser (514 nm, 5 mW) focused onto a microsized spot (1 μm). Electron paramagnetic resonance (EPR) spectra were taken on a JES-TE200 (JEOL) by applying an X-band (9.43 GHz, 1.5 mW) microwave and sweeping magnetic field at RT.

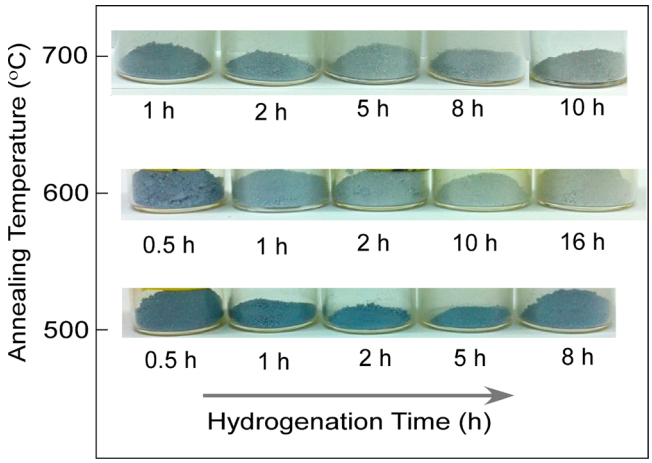

Figure 1. Photograph of our H-$aTiO_2$ samples prepared with a H_2 gas flow at temperatures of 500−700 °C. Gradual changes in color from blue to gray to a different degree are observed, depending on annealing temperatures and annealing time.

Photoactivity Measurements. To evaluate the photocatalytic activity of H-$aTiO_2$ and $aTiO_2$, a photodegradation of methylene blue (MB) over TiO_2 under a UV illumination (6 W, 365 nm) was carried out in an aqueous solution at RT. The initial concentration of MB and TiO_2 catalyst was set to 0.01 mM and 0.006 g/L, respectively. The photocatalytic reactions were initiated after equilibrium was achieved in the aqueous solution in a dark place. The concentration of MB was measured from the absorbance at 659 nm using a UV−vis spectrophotometer (Scinco, S-2130).

3. RESULTS AND DISCUSSION

The as-synthesized $aTiO_2$ (a white powder) changed its color to a strong blue at the early stage (0.5−1 h) of hydrogenation. With longer hydrogenation treatments (up to 8−16 h), the blue color gradually changed into gray (Figure 1). The color change also showed a strong dependence on the annealing temperature. The blue color was maintained up to a longer time at 500 °C, but it readily changed to a pale gray at 600 °C. The color changes here are due to the reduction of $aTiO_2$ during the cycles of hydrogenation. After the hydrogenation, the color (either blue or gray) remained unchanged for several months at ambient conditions, indicating the stability of the defects.

The TEM images of $aTiO_2$ in Figure 2 show that the crystal has the shape of a nanosheet with large square-shaped (001) planes with a width of 50−70 nm and a thickness of 5−9 nm (Supporting Information Figure S1a and b). After hydrogenation, we note that the thin, planar, square shape of $aTiO_2$ has changed into the one with an enhanced thickness (Figure 2). H-$aTiO_2$ nanocrystals in Figure 2 all show a crystal shape of a truncated tetragonal bipyramid with enlarged {101} facets (see H-$aTiO_2$ in Figure 2). During such a shape change upon hydrogenation, the anatase phase of $aTiO_2$ is found to be largely observed up to 700 °C (Figure 2). In addition to the anatase phase, however, the rutile phase is also detected at 700 °C (Supporting Information Figure S1d). The phase transformation into rutile at 700 °C is further discussed from the XRD measurements in Figure 3.

The hydrogenation may eliminate F atoms left on the surface of $aTiO_2$[22] as well as surface oxygen atoms, leaving the surface covered with O−H or Ti−H.[28] Such changes at the surface increase the surface free energies of (101) and (001) surfaces of

dx.doi.org/10.1021/cs4005776 | ACS Catal. 2013, 3, 2479−2486

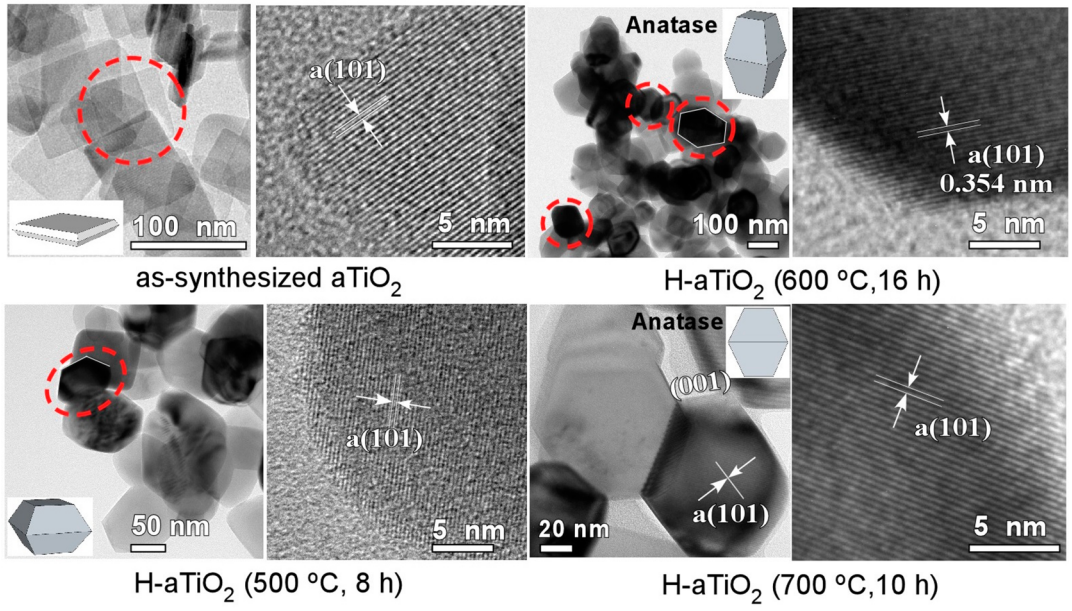

Figure 2. TEM images of $aTiO_2$ and H-$aTiO_2$ prepared at temperatures of 500−700 °C. A crystalline anatase phase with the well-defined anatase (101) spacing is identified for all H-$aTiO_2$. In addition, a thin nanosheet-shaped $aTiO_2$ with large {001} facets changes its shape into a truncated tetragonal bipyramid with enlarged {101} facets upon hydrogenation (H-$aTiO_2$).

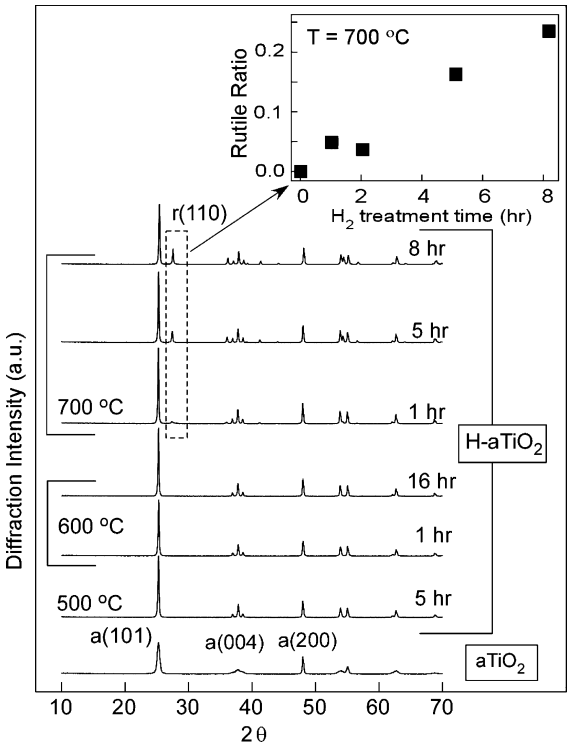

Figure 3. XRD spectra of $aTiO_2$ and H-$aTiO_2$ prepared at temperatures of 500−700 °C. A crystalline anatase phase is maintained upon the hydrogenation up to 700 °C. In addition, a rutile phase is observed to increase at 700 °C with increasing hydrogenation time. The rutile-to-anatase ratio of H-$aTiO_2$ prepared at 700 °C (in the inset) is calculated from the intensities of the anatase (101) and rutile (110) peaks.

H-$aTiO_2$ compared with those of $aTiO_2$, which may drive a shape change into the one with enlarged {101} facets at elevated temperatures as a result of the reversed surface free energies of hydrogenated (101) and (001) surfaces.[10]

Further details of the change in the bulk phase investigated from XRD are shown in Figure 3. The anatase phase of $aTiO_2$ is confirmed to be preserved upon hydrogenation at 500−600 °C. The sharp anatase (101) peak of H-$aTiO_2$ compared with that of $aTiO_2$ (Figure 3) originates from the shape change (TEM images of Figure 2) into a truncated bipyramid with extended {101} facets. No measurable shift in the XRD peak position of the anatase phase is observed, implying no significant hydrogen-induced distortion in the bulk anatase phase under our hydrogenation conditions.

The shape (or a size) change observed in the TEM image (Figure 2) is also reflected in the intensity variations of anatase (004) and (200) peaks in XRD (Figure 3) upon hydrogenation. An enhancement of the (004) peak compared with the (200) reflects the increased thickness along the [001] direction.[10,37] A little change in the (200) peak suggests the lateral size of the nanosheet is unchanged.

In addition to the anatase phase, hydrogenation at 700 °C induces additional XRD peaks that are assigned to the rutile phase (see Figure 3 as well as Supporting Information Figure S1). The unambiguous rutile (110) peak at $2\theta = 27.4°$ increases with increasing hydrogenation time (as shown in the inset of Figure 3). Early reports indicate that the anatase-to-rutile phase transition of anatase TiO_2 occurs upon annealing above 550 °C.[38] In our case, a higher temperature (700 °C) is required to induce the phase transition; this is attributed to the effect of hydrogenation in suppressing the phase transition from anatase to rutile, as has been predicted earlier.[39]

UV−vis DR spectra of H-$aTiO_2$ are shown in Figure 4. A sharp increase in the absorbance at around 400 nm (a black line in Figure 4a) is due to the band gap of anatase TiO_2. The Kubelka−Munk function applied to the spectrum indicates an indirect band gap of ∼3.2 eV. DR spectra of H-$aTiO_2$ prepared at 500−600 °C all show the absorbance rising at around the similar photon energies (Figure 4a). The band gap of the H-$aTiO_2$ is measured as in the range of 3.0−3.2 eV (Figure 4b) without any meaningful shift, which is consistent with the result

dx.doi.org/10.1021/cs4005776 | ACS Catal. 2013, 3, 2479−2486

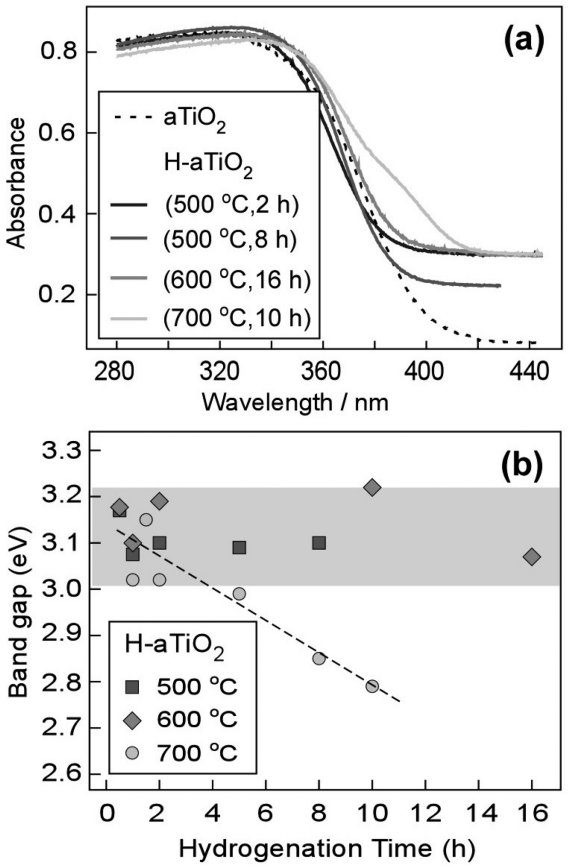

Figure 4. (a) UV−vis DR spectra of $aTiO_2$ and H-$aTiO_2$ nanosheets are compared. (b) Band gap is calculated from the Kubella−Munk function applied to the DR spectra in panel a and is plotted against the H_2 annealing time. The band gap is found to be in the range of 3.0−3.2 eV (see the gray area in panel b) for H-$aTiO_2$ prepared at 500−600 °C, but it decreases below 3.0 eV (see the dashed line in panel b) for $aTiO_2$ prepared at 700 °C.

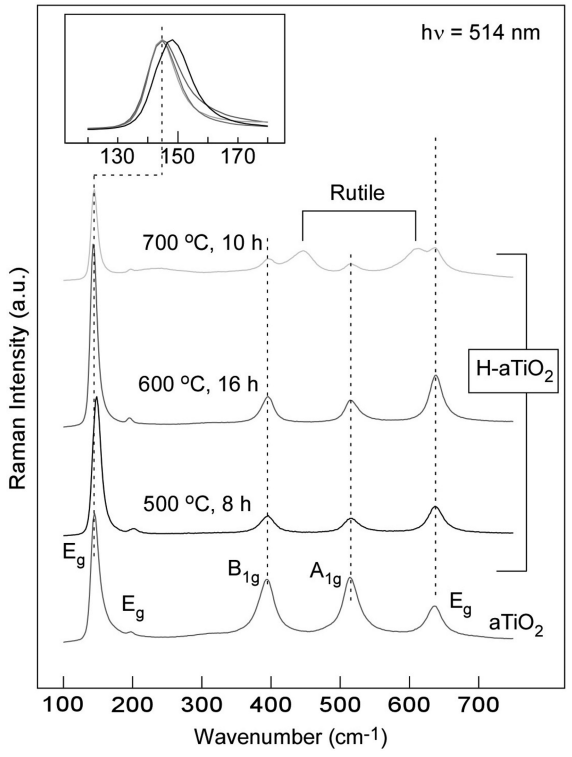

Figure 5. Raman spectra of $aTiO_2$ and H-$aTiO_2$ are compared. Characteristic four major Raman modes of the anatase phase are observed for all TiO_2 samples ($aTiO_2$ and H-$aTiO_2$). Raman modes due to the rutile phase are observed only for H-$aTiO_2$ prepared at 700 °C. The E_g band is normalized and compared in the inset and is observed to be blue-shifted only for H-$aTiO_2$ hydrogenated at 500 °C.

in Figure 3; the anatase phase is preserved upon the hydrogenation treatment up to 600 °C. The hydrogenation at 700 °C, however, results in the absorption edge farther shifting down to lower energies below 3.0 eV (see the dashed line in Figure 4b) with increasing hydrogenation time. The decrease in the band gap is without any doubt attributed to the growth of rutile phase with a band gap of 3.0 eV, which is in contact with anatase. This can induce band gap narrowing as a result of the characteristic band alignment at the anatase/rutile interface[40] and the formation of the interfacial defects between the anatase and rutile phases.[40,41]

Raman spectra of $aTiO_2$ in Figure 5 show well-resolved distinct peaks at 144, 394, 514, and 637 cm^{-1} and a small peak at 197 cm^{-1}. All of these features are due to Raman-active modes of the anatase phase of TiO_2.[38] We see that the spectra of H-$aTiO_2$ hydrogenated at 500 and 600 °C also show these Raman modes again because the anatase phase is preserved during the hydrogenation (see XRD results in Figure 3). A shoulder at around 320 cm^{-1} is also noted for $aTiO_2$ and H-$aTiO_2$.[31] In addition, the E_g mode at 144 cm^{-1} shifts to 149 cm^{-1} only for H-$aTiO_2$ hydrogenated at 500 °C (see the inset of Figure 5). No other peak shift is observed, except an enhancement in the intensities of E_g modes at 144 and 637 cm^{-1} compared to the other modes for H-$aTiO_2$.

The rutile phase of H-$aTiO_2$ prepared at 700 °C (XRD in Figure 3) is also confirmed from additional Raman features at 445 and 612 cm^{-1} (the Raman features of the rutile phase).[38,42] A reduced ratio of anatase phase is reflected from the obvious decrease of the Raman modes associated with the anatase phase (especially the intensity at 144 cm^{-1}).

An enhancement in the intensities of E_g modes at 144 and 637 cm^{-1} compared with the other modes (A_{1g} and B_{1g}) for H-$aTiO_2$ reflects a change in the ratio of {001} facets to others.[37] Larger {001} facets decrease the intensity of the E_g peaks in the Raman spectra as a result of the reduced number of the symmetric stretching vibration modes of O−Ti−O, whereas the A_{1g} and B_{1g} peaks in the Raman spectra increase due to the increased number of the symmetric bending vibration and the antisymmetric bending vibration modes of O−Ti−O.[37] Thus, the enhanced E_g mode of H-$aTiO_2$ (Figure 5) reflects a decreased percentage of {001} facets, which is consistent with the TEM images (Figure 2).

The shift of E_g mode at 144 cm^{-1} to 149 cm^{-1} observed only for H-$aTiO_2$ hydrogenated at 500 °C, not at 600−700 °C, (the inset of Figure 5) may be due to a size change,[43,44] a lattice disorder introduced from hydrogenation, or defects such as oxygen vacancies.[1,27] In our case, the changing colors of H-$aTiO_2$ from white ($aTiO_2$) to blue (or gray) (Figure 1) suggest that the hydrogenation introduces defects into the bulk (or surface) of the TiO_2 nanocrystals, which can induce a blue-shift of the E_g mode. At the same time, we also note a shape (as well as a size) change (TEM images of Figure 2) with an enhanced crystallinity in the bulk (XRD in Figure 3) for H-$aTiO_2$. An increase in the size associated with the shape change of $aTiO_2$

dx.doi.org/10.1021/cs4005776 | ACS Catal. 2013, 3, 2479−2486

upon the hydrogenation may induce a red-shift of the Raman peak.[44,45] Thus, the peak shift of ~5 cm^{-1} observed only for $aTiO_2$–H_2 prepared at 500 °C, not at higher temperatures, is likely to be a compensating effect of size[37] and the lattice defects[46] during hydrogenation at different temperatures (500–700 °C).

Figure 6 shows EPR spectra of $aTiO_2$ and H-$aTiO_2$ nanocrystals. $aTiO_2$ does not show any distinct absorption

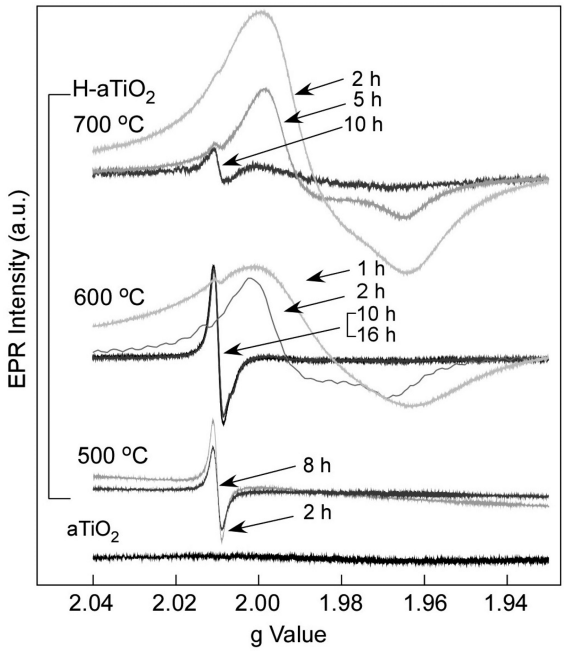

Figure 6. Room-temperature X-band EPR spectra of as-synthesized $aTiO_2$ and H-$aTiO_2$ prepared at 500, 600, and 700 °C, respectively.

peak under our EPR measurement conditions at RT. On the other hand, all H-$aTiO_2$ show unambiguously intense EPR signals at around g = 1.98 and 2.01. At 500 °C, we observe only a single resolved EPR signal at g = 2.01 with varying intensities, depending on the annealing time. This signal, which can be related to the intense blue color, remains up to a longer hydrogenation treatment time (up to 8 h). At higher temperatures (600 and 700 °C), another broad absorption peak is observed at g = 1.96–1.99 (which is assigned to a paramagnetic Ti^{3+} center)[21] in addition to the small shoulder at g = 2.01, especially for H-$aTiO_2$ hydrogenated for only 1–2 h. With longer hydrogenation treatments, the EPS signals at g = 1.96–1.99 diminish, and the signal at g = 2.01 increases.

The broad line shape of the Ti^{3+}-related EPR signal originates from the short relaxation time of the Ti^{3+} species.[47] Recent studies have shown that various shapes of the Ti^{3+}-related EPR signals at g = 1.96–1.99 can be induced by H_2 treatments of anatase TiO_2,[28] and N- or F-doped TiO_2.[48]

The signal at g = 2.01 is usually attributed to O^- species. Surface O^- species may be generated from the interaction of O_2 with the surface Ti^{3+} species associated with surface oxygen vacancies.[5,48,49] Hydrogenation of $aTiO_2$ removes trace of surface F atoms left on the surfaces of $aTiO_2$ nanocrystals during the preparation.[28] In addition, the surface O atoms are eliminated from the surface via the formation of surface OH species, which desorb from the surface as H_2O at elevated temperatures above 500 K.[50] This leaves surface oxygen vacancies with Ti^{3+} species and Ti^{3+} interstitials on the surface, which subsequently interact with O_2 from the air, producing O_2^- initially, then O^- species.[28] Excess surface charges associated with Ti^{3+} species facilitate the formation of the surface O^- species from O_2^-, and the surface O^- species are stabilized by the electrophilic nature of oxygen and the coulomb interaction with Ti^{4+} sites.[51,52]

However, the assignment of O^- species to the EPR signal at g = 2.01 may not be so straightforward because the measured near-isotropic shape of the peak is quite different from the expected anisotropic nature of the O^- species.[49] A possible reason for the anomalous near-isotropic shape may be attributed to heterogeneity of the surface sites. In addition, a contribution of electrons that may be trapped in oxygen vacancy clusters may also overlap with the O^--related EPR signal to change the overall shape. Thus, the EPR signal may be assigned to the surface O^- species,[28,49] with a possible contribution of vacancy-trapped electrons.

In addition to the surface defects, hydrogenation also induce defects in the bulk,[53] such as Ti^{3+} interstitials and oxygen vacancies.[54] Depletion of surface O atoms during hydrogenation leaves the TiO_2 crystals oxygen-deficient. The charge balance requires the excess charges to be left in forms of Ti^{3+} defects that are located in lattice sites adjacent to the oxygen vacancies or in interstitial sites (Ti^{3+} interstitials). Diffusion of such Ti^{3+} defects (oxygen vacancies and Ti^{3+} interstitials) into/from the bulk occurs readily at 500–700 °C,[54] along with kinetically limited changes in the overall size, shape (Figure 2), crystallinity, and bulk phases (from anatase into rutile) (Figure 3). This would result in a gradual change in the concentration and the distribution of such defects.

Preferential migration of bulk oxygen vacancies to the surface is expected to form more stable surface oxygen vacancies.[55,56] Such a change is probed from a variation in the characteristic EPR signals as measured for our H-$aTiO_2$ in the present study. The relative population between the two kinds of defects may vary, depending on the annealing temperature,[54] and maximum Ti^{3+} concentration is achieved at the early stage of hydrogenation at 600 and 700 °C, as can be seen from the strong Ti^{3+} EPR signals in Figure 6.

At lower temperatures (~ 500 °C), oxygen vacancies are preferentially formed on the surface.[49] The surface oxygen vacancies with adjacent Ti^{3+} sites, once exposed to air, would interact with molecular O_2, to produce O_2^-, which can further react to leave O^- species trapped in surface oxygen vacancies.

Longer hydrogenation (>5 h) at 600–700 °C induces the attenuation of the Ti^{3+} EPR signals with enhanced O^--related EPR signal, which indicates a change in the type/concentration of defects in the bulk/surface of H-$aTiO_2$. Localized bulk Ti^{3+} defects may diffuse to the surface or are collected at the grain boundaries,[36,57] which is attributed to the reduced Ti^{3+}-related EPR signals. An enhanced O^--related EPR signal upon the prolonged hydrogenation treatment explains that bulk Ti^{3+} defects diffuse into the surface to form surface oxygen vacancies, which would later interact with O_2 to leave O^- species on the surface, thus explaining the observed O^- EPR signal.

The photoactivity of H-$aTiO_2$ is compared from the photodegradation rate of MB under UV irradiation in Figure 7. The concentration ratio (C/C_0) of MB plotted against UV irradiation time in the presence of the $aTiO_2$ (H-$aTiO_2$) catalysts shows a pseudo-first-order kinetics to the MB concentration. Interestingly, the figure shows that our H-$aTiO_2$ nanocrystals can have either a higher or a lower

dx.doi.org/10.1021/cs4005776 | ACS Catal. 2013, 3, 2479–2486

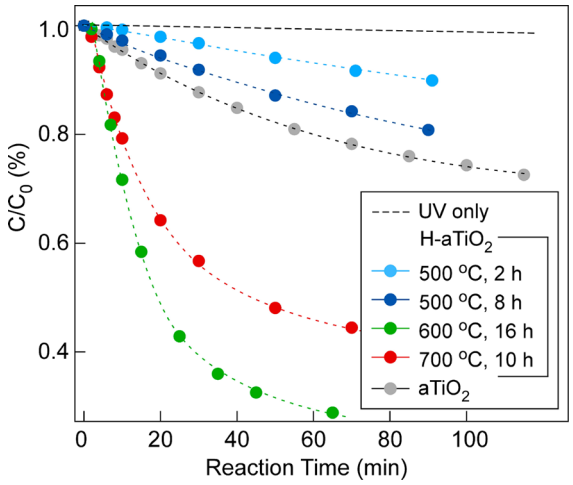

Figure 7. Photodegradation of methylene blue (MB) under UV irradiation is compared. Under the hydrogenation condition employed in this study, our H-aTiO_2 nanocrystals are found to have either higher or lower photoactivity compared with aTiO_2.

photodegradation rate than aTiO_2, depending on the annealing temperature. H-aTiO_2 prepared at 500 °C has lower reaction rates than as-synthesized aTiO_2, whereas hydrogenation at 600−700 °C, especially for those H_2 treated for 10−16 h, induces higher photodegradation rates.

The photodegradation reaction rates of all our H-aTiO_2 nanocrystals (Figure 7) are compared with each other by plotting photoactivity or rate constant (k, min^{-1}) against the hydrogenation time in Figure 8. Here, we find that the

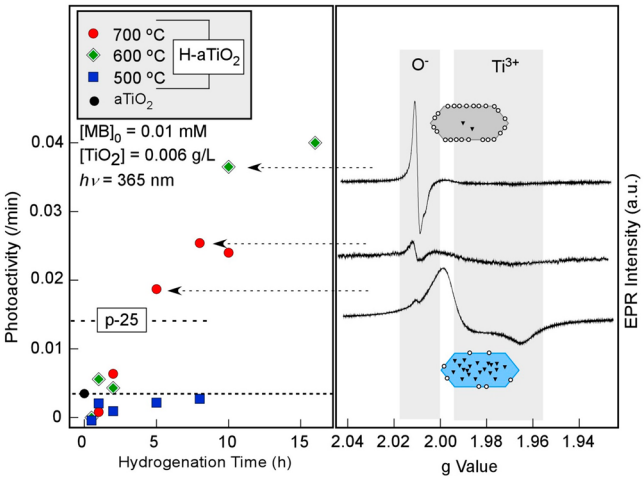

Figure 8. Photoactivities (k, min^{-1}) and EPR spectra of H-aTiO_2 are shown together against hydrogenation time and temperatures.

photoactivity of H-aTiO_2 varies depending not only on the annealing temperature but also on the hydrogenation time. Compared with the photoactivity of aTiO_2 (0.004 min^{-1}), H-aTiO_2 prepared at 500 °C shows lower photoactivity; it increases proportional to the hydrogenation time, but is still lower than aTiO_2 up to 8 h of hydrogenation time. However, H-aTiO_2 nanocrystals prepared at 600 and 700 °C show drastically enhanced photoactivities when they are hydrogenated for a longer time (>5 h). About 10 times higher photoactivities are measured for H-aTiO_2 hydrogenated at 600 °C when they are treated longer than 10 h.

Figure 8 also shows how EPR spectra of H-aTiO_2 nanocrystals change as the photoactivity is enhanced. Strong EPR signals at g = 1.96−1.99, indicative of Ti^{3+} species in the bulk (or surface), are observed for H-aTiO_2 with better photoactivities than aTiO_2. In addition, even better (5−10 times higher) photoactivity is achieved when the Ti^{3+}-related EPR signals decrease and the O^--related EPR signal at g = 2.01 is enhanced. This result clearly shows that the photoactivity of TiO_2 has a strong correlation with the varying nature of defects in TiO_2 nanocrystals, which can be determined by a surface-to-bulk defect density ratio and absolute concentration and distribution of Ti^{3+} and oxygen vacancies.

Our results confirm that higher Ti^{3+} concentration measured in the EPR spectra is beneficial in enhancing the photoactivity compared with aTiO_2, which may be in part due to the role of Ti^{3+} species as hole scavengers. In addition, oxygen vacancies on the surface would act as O_2 binding sites and electron scavengers,[5] thus contributing to enhanced photoactivity.

A new insight gained in this study is that a further (dramatic) enhancement in photoactivity is obtained for H-aTiO_2 nanocrystals hydrogenated at 600 °C, which show EPR spectra characterized by a decrease of Ti^{3+} and an increase of surface O^-. At the early stage of hydrogenation, surface oxygen atoms are removed from the surface by a recombinative H_2O desorption, which leaves the crystal oxygen-deficient (or reduced). Thus, Ti^{3+} defects can be formed in the bulk of the reduced TiO_2 in the forms of oxygen vacancies and Ti^{3+} interstitials. As the hydrogenation proceeds further, such Ti^{3+} defects may diffuse toward the surface and transform into surface oxygen vacancies during the hydrogenation process. The surface oxygen vacancies interact with molecular O_2 at ambient conditions to produce surface O_2^-, which may dissociate into O^-. The defects such as oxygen vacancy clusters (or oxygen vacancy associates) may be formed on the surface or at the grain boundaries of anatase and rutile as a result of grain boundary migration, which promotes the separation of electron−hole pairs under irradiation, thus, improving the photocatalytic activity remarkably.[36,57]

The question then is why the H-aTiO_2 nanocrystals prepared at 500 °C show lower photoactivities than aTiO_2. The origin for such a difference may be found from the observation that they have only surface O^- type defects and no detectable EPR signal that can be assigned to Ti^{3+} from the very early stage of hydrogenation. A difference in the detailed shape of the EPR feature at g = 2.0 between the highly photoactive H-aTiO_2 (600 °C) and the less photoactive H-aTiO_2 (500 °C) may also reflect a difference in the distribution of such defects on the surface, for example, a clustered nature of O^- species. Thus, our results show that a kinetically controlled hydrogenation condition can induce such a varying degree of defect concentration and distribution in TiO_2 nanocrystals[30] by adjusting experimental parameters such as the annealing temperature and the annealing time.

Our studies show that the color change from blue to gray (Figure 1) is also used as an indicator for higher photoactivity. The photoactivity is enhanced (Figure 8) when the color changes from blue to gray (Figure 1). A strong blue color, in our case, decreases the photoactivity dramatically, even compared with that of aTiO_2 (Figure 8). The color change to gray and a subsequent change in photoactivity after hydrogenation turn out to depend on kinetic parameters such as a cooling rate and process time.[27,58]

dx.doi.org/10.1021/cs4005776 | ACS Catal. 2013, 3, 2479−2486

The hydrogenation-induced shape change from a nanosheet into a truncated tetragonal bipyramid (Figure 2) may have a negative effect on the resulting photoactivity because the change is toward decreasing the area of {001} facets with a higher photoactivity.[12] In addition, such a shape change occurs at all temperatures, whereas the difference in photoactivity is observed between 500 and 600−700 °C (Figure 8). Thus, the shape change upon hydrogenation is less likely to act as an origin of the observed enhancement in photoactivity of H-aTiO_2.

Remanent F atoms on the surface of aTiO_2 may enhance the photoactivity of anatase TiO_2.[25] We also detected F species on aTiO_2 (but not on H-aTiO_2) in our XPS measurements (not shown here) as other groups.[22,28,48] Although the F atoms on TiO_2 surface may enhance[59,60] or decrease[22] the photoactivity of aTiO_2, the decrease in photoactivity observed at the very initial stage of hydrogenation (especially at 500 °C) may in part originate from the loss of F atoms from the surface during hydrogenation.[28,48] Elimination of F atoms during hydrogenation may also generate surface Ti−H bonds as a result of a direct interaction between five-coordinated Ti atoms and H_2,[28,31] which may act in favor of enhancing the photoactivity, as has been observed, especially in our case of prolonged hydrogenation.

The band gap narrowing is marginal under our controlled hydrogenation condition of 500−600 °C, and only a meaningful decrease in the band gap down to 2.8 eV is observed for the hydrogenation at 700 °C with an increasing rutile ratio. The influence of the enhanced photoabsorption due to the reduced band gap is marginal in our case because the photon energy of the UV lamp (∼3.4 eV) used in this study is higher than the band gap of our H-aTiO_2 prepared. Here, the photoactivity is not limited by the photon absorption; instead, the measured enhancement in the photoactivity of H-aTiO_2 prepared at 600−700 °C can be attributed to the relative ease with which photogenerated hot electrons and holes can be delivered to the surface without being destroyed by electron−hole recombination processes. The presence of mixed phases of anatase and rutile has been shown to generate interfacial defects that are beneficial in minimizing the recombination rate[41,61] and in enhancing photoactivities.[41,62] This fact is also confirmed in our results from the reduced band gap (Figure 4b) and the enhanced photoactivity (Figure 8) of H-aTiO_2 prepared at 700 °C. Even higher photoactivities for the case of 600 °C, achieved with longer hydrogenation time, suggest that the thermal hydrogenation condition of 600 °C induces a progressive change in the distribution and concentration of defects in the bulk as well as on the surface (see the EPR spectra in Figure 6) toward a direction that minimizes (maximizes) the recombination rate (the photoactivity) (see the results of photoactivity measurements in Figure 8).

4. CONCLUSIONS

Hydrogenation of anatase TiO_2 nanosheets performed under a H_2 gas flow in the temperature range of 500−700 °C induces changes in size, shape, bulk phase, band gap, and defect concentration and distribution. Among such changes, a nonuniform distribution of defects between the surface and the bulk is found to play a central role in controlling the photoactivity. Under our experimental conditions, hydrogenation at 600 °C is found to induce a large number of Ti^{3+} defects in the beginning and, eventually, O^- as a major species on the surface after prolonged hydrogenation. This change in the distribution of defects in the surface and the bulk is attributed to the origin of the dramatic enhancement of photoactivity. Our results show that a controlled hydrogenation combined with proper characterization of defects can further enhance our understanding of the role of defects in photocatalytic properties of oxide nanocrystals.

■ ASSOCIATED CONTENT

Supporting Information

Figure S1 shows additional images of the as-synthesized aTiO_2 showing the shape and the size distribution of aTiO_2 nanosheets and TEM images of H-aTiO_2 nanocrystals hydrogenated at 700 °C showing the anatase (c) and rutile (d) phases. This material is available free of charge via the Internet at http://pubs.acs.org.

■ AUTHOR INFORMATION

Corresponding Author

*Phone: 82-31-219-2896. Fax: 82-31-219-2969. E-mail: yukwonkim@ajou.ac.kr.

Notes

The authors declare no competing financial interest.

■ ACKNOWLEDGMENTS

This research was supported by the Basic Science Research Program through the National Research Foundation of Korea (NRF) funded by the Ministry of Education, Science and Technology (NRF-2010-0010780, NRF-2012R1A1A2007641).

■ REFERENCES

(1) Chen, X.; Mao, S. S. *Chem. Rev.* **2007**, *107*, 2891.
(2) Fujishima, A.; Zhang, X.; Tryk, D. A. *Surf. Sci. Rep.* **2008**, *63*, 515.
(3) Diebold, U. *Surf. Sci. Rep.* **2003**, *48*, 53.
(4) Ni, M.; Leung, M. K. H.; Leung, D. Y. C.; Sumathy, K. *Renewable Sustainable Energy Rev.* **2007**, *11*, 401.
(5) Thompson, T.; Yates, J., Jr. *Top. Catal.* **2005**, *35*, 197.
(6) Zheng, Z.; Huang, B.; Meng, X.; Wang, J.; Wang, S.; Lou, Z.; Wang, Z.; Qin, X.; Zhang, X.; Dai, Y. *Chem. Commun.* **2013**, *49*, 868.
(7) Zhang, J.; Xi, J.; Ji, Z. *J. Mater. Chem.* **2012**, *22*, 17700.
(8) Yu, J.; Dai, G.; Xiang, Q.; Jaroniec, M. *J. Mater. Chem.* **2011**, *21*, 1049.
(9) Zhang, H.; Liang, Y.; Wu, X.; Zheng, H. *Mater. Res. Bull.* **2012**, *47*, 2188.
(10) Yang, H. G.; Sun, C. H.; Qiao, S. Z.; Zou, J.; Liu, G.; Smith, S. C.; Cheng, H. M.; Lu, G. Q. *Nature* **2008**, *453*, 638.
(11) Han, X.; Kuang, Q.; Jin, M.; Xie, Z.; Zheng, L. *J. Am. Chem. Soc.* **2009**, *131*, 3152.
(12) Wang, Z.; Lv, K.; Wang, G.; Deng, K.; Tang, D. *Appl. Catal., B* **2010**, *100*, 378.
(13) Zheng, Z.; Huang, B.; Qin, X.; Zhang, X.; Dai, Y.; Jiang, M.; Wang, P.; Whangbo, M.-H. *Chem.—Eur. J.* **2009**, *15*, 12576.
(14) Sun, F.; Zhou, W.; Tian, G.; Pan, K.; Miao, X.; Li, Y.; Zhang, G.; Li, T.; Fu, H. *ChemCatChem* **2012**, *4*, 844.
(15) Joo, J. B.; Zhang, Q.; Dahl, M.; Zaera, F.; Yin, Y. *J. Mater. Res.* **2013**, *28*, 362.
(16) Zhao, Y.; Zhao, Q.; Li, X.; Hou, Y.; Zou, X.; Wang, J.; Jiang, T.; Xie, T. *Mater. Lett.* **2012**, *66*, 308.
(17) Deiana, C.; Minella, M.; Tabacchi, G.; Maurino, V.; Fois, E.; Martra, G. *Phys. Chem. Chem. Phys.* **2013**, *15*, 307.
(18) Aprile, C.; Corma, A.; Garcia, H. *Phys. Chem. Chem. Phys.* **2008**, *10*, 769.
(19) Wu, N.; Wang, J.; Tafen, D. N.; Wang, H.; Zheng, J.-G.; Lewis, J. P.; Liu, X.; Leonard, S. S.; Manivannan, A. *J. Am. Chem. Soc.* **2010**, *132*, 6679.

(20) Kong, M.; Li, Y.; Chen, X.; Tian, T.; Fang, P.; Zheng, F.; Zhao, X. *J. Am. Chem. Soc.* **2011**, *133*, 16414.
(21) Zuo, F.; Wang, L.; Wu, T.; Zhang, Z.; Borchardt, D.; Feng, P. *J. Am. Chem. Soc.* **2010**, *132*, 11856.
(22) Pan, J.; Liu, G.; Lu, G. Q.; Cheng, H.-M. *Angew. Chem., Int. Ed.* **2011**, *50*, 2133.
(23) Liu, S.; Yu, J.; Jaroniec, M. *J. Am. Chem. Soc.* **2010**, *132*, 11914.
(24) Xie, S.; Han, X.; Kuang, Q.; Fu, J.; Zhang, L.; Xie, Z.; Zheng, L. *Chem. Comm* **2011**, *47*, 6722.
(25) Kim, H.; Choi, W. *Appl. Catal., B* **2007**, *69*, 127.
(26) Chen, X.; Liu, L.; Yu, P. Y.; Mao, S. S. *Science* **2011**, *331*, 746.
(27) Naldoni, A.; Allieta, M.; Santangelo, S.; Marelli, M.; Fabbri, F.; Cappelli, S.; Bianchi, C. L.; Psaro, R.; Dal Santo, V. *J. Am. Chem. Soc.* **2012**, *134*, 7600.
(28) Wei, W.; Yaru, N.; Chunhua, L.; Zhongzi, X. *RSC Adv.* **2012**, *2*, 8286.
(29) Wang, G.; Wang, H.; Ling, Y.; Tang, Y.; Yang, X.; Fitzmorris, R. C.; Wang, C.; Zhang, J. Z.; Li, Y. *Nano Lett.* **2011**, *11*, 3026.
(30) Nowotny, M. K.; Sheppard, L. R.; Bak, T.; Nowotny, J. *J. Phys. Chem. C* **2008**, *112*, 5275.
(31) Zheng, Z.; Huang, B.; Lu, J.; Wang, Z.; Qin, X.; Zhang, X.; Dai, Y.; Whangbo, M.-H. *Chem. Commun.* **2012**, *48*, 5733.
(32) Justicia, I.; Ordejón, P.; Canto, G.; Mozos, J. L.; Fraxedas, J.; Battiston, G. A.; Gerbasi, R.; Figueras, A. *Adv. Mater.* **2002**, *14*, 1399.
(33) Zou, X.; Liu, J.; Su, J.; Zuo, F.; Chen, J.; Feng, P. *Chem.—Eur. J.* **2013**, *19*, 2866.
(34) Leshuk, T.; Parviz, R.; Everett, P.; Krishnakumar, H.; Varin, R. A.; Gu, F. *ACS Appl. Mater. Interfaces* **2013**, *5*, 1892.
(35) Lu, J.; Dai, Y.; Jin, H.; Huang, B. *Phys. Chem. Chem. Phys.* **2011**, *13*, 18063.
(36) Yan, J.; Wu, G.; Guan, N.; Li, L.; Li, Z.; Cao, X. *Phys. Chem. Chem. Phys.* **2013**, *15*, 10978.
(37) Tian, F.; Zhang, Y.; Zhang, J.; Pan, C. *J. Phys. Chem. C* **2012**, *116*, 7515.
(38) Zhang, J.; Li, M.; Feng, Z.; Chen, J.; Li, C. *J. Phys. Chem. B* **2006**, *110*, 927.
(39) Barnard, A. S.; Curtiss, L. A. *Nano Lett.* **2005**, *5*, 1261.
(40) Scanlon, D. O.; Dunnill, C. W.; Buckeridge, J.; Shevlin, S. A.; Logsdail, A. J.; Woodley, S. M.; Catlow, C. R. A.; Powell, M. J.; Palgrave, R. G.; Parkin, I. P.; Watson, G. W.; Keal, T. W.; Sherwood, P.; Walsh, A.; Sokol, A. A. *Nat. Mater.* **2013**, *12*, 798.
(41) Hurum, D. C.; Agrios, A. G.; Gray, K. A.; Rajh, T.; Thurnauer, M. C. *J. Phys. Chem. B* **2003**, *107*, 4545.
(42) Zhang, W. F.; He, Y. L.; Zhang, M. S.; Yin, Z.; Chen, Q. *J. Phys. D: Appl. Phys.* **2000**, *33*, 912.
(43) Choi, H. C.; Jung, Y. M.; Kim, S. B. *Vib. Spectrosc.* **2005**, *37*, 33.
(44) Gupta, S. K.; Desai, R.; Jha, P. K.; Sahoo, S.; Kirin, D. *J. Raman Spectrosc.* **2010**, *41*, 350.
(45) Sahoo, S.; Arora, A. K.; Sridharan, V. *J. Phys. Chem. C* **2009**, *113*, 16927.
(46) Liu, G.; Yang, H. G.; Wang, X.; Cheng, L.; Lu, H.; Wang, L.; Lu, G. Q.; Cheng, H.-M. *J. Phys. Chem. C* **2009**, *113*, 21784.
(47) Czoska, A. M.; Livraghi, S.; Chiesa, M.; Giamello, E.; Agnoli, S.; Granozzi, G.; Finazzi, E.; Valentin, C. D.; Pacchioni, G. *J. Phys. Chem. C* **2008**, *112*, 8951.
(48) Wang, W.; Lu, C.; Ni, Y.; Su, M.; Xu, Z. *Appl. Catal., B* **2012**, *127*, 28.
(49) Strunk, J.; Vining, W. C.; Bell, A. T. *J. Phys. Chem. C* **2010**, *114*, 16937.
(50) Henderson, M. A. *Langmuir* **1996**, *12*, 5093.
(51) Che, M.; Tench, A. J. *Adv. Catal.* **1983**, *32*, 1.
(52) Che, M.; Tench, A. J. *Adv. Catal.* **1982**, *31*, 77.
(53) Haerudin, H.; Bertel, S.; Kramer, R. *J. Chem. Soc. Trans.* **1998**, *94*, 1481.
(54) Liu, H.; Ma, H. T.; Li, X. Z.; Li, W. Z.; Wu, M.; Bao, X. H. *Chemosphere* **2003**, *50*, 39.
(55) Jug, K.; Nair, N. N.; Bredow, T. *Phys. Chem. Chem. Phys.* **2005**, *7*, 2616.
(56) Pan, J. M.; Maschhoff, B. L.; Diebold, U.; Madey, T. E. *J. Vac. Sci. Technol., A* **1992**, *10*, 2470.
(57) Jiang, X.; Zhang, Y.; Jiang, J.; Rong, Y.; Wang, Y.; Wu, Y.; Pan, C. *J. Phys. Chem. C* **2012**, *116*, 22619.
(58) Chiesa, M.; Paganini, M. C.; Livraghi, S.; Giamello, E. *Phys. Chem. Chem. Phys.* **2013**, *15*, 9435.
(59) Liu, G.; Sun, C.; Yang, H. G.; Smith, S. C.; Wang, L.; Lu, G. Q.; Cheng, H.-M. *Chem. Commun.* **2010**, *46*, 755.
(60) Yu, J.; Wang, W.; Cheng, B.; Su, B.-L. *J. Phys. Chem. C* **2009**, *113*, 6743.
(61) Li, G.; Gray, K. A. *Chem. Phys.* **2007**, *339*, 173.
(62) Zhao, H.; Liu, L.; Andino, J. M.; Li, Y. *J. Mater. Chem. A* **2013**, *1*, 8209.